

Secrecy Rate Maximization for Intelligent Reflecting Surface Assisted MIMOME Wiretap Channels

Anshu Mukherjee, Vaibhav Kumar, and Le-Nam Tran

School of Electrical and Electronic Engineering, University College Dublin, Belfield, Dublin 4, Ireland

Email: anshu.mukherjee@ucdconnect.ie; vaibhav.kumar@ieee.org; nam.tran@ucd.ie

Abstract—Intelligent reflecting surface (IRS) has gained tremendous attention recently as a disruptive technology for beyond 5G networks. In this paper, we consider the problem of secrecy rate maximization for an IRS-assisted Gaussian multiple-input multiple-output multi-antenna-eavesdropper (MIMOME) wiretap channel (WTC). In this context, we aim to jointly optimize the input covariance matrix and the IRS phase shifts to maximize the achievable secrecy rate of the considered system. To solve the formulated problem which is non-convex, we propose an iterative method based on the block successive maximization (BSM), where *each iteration is done in closed form*. More specifically, we maximize a lower bound on the achievable secrecy rate to update the input covariance matrix for fixed phase shifts, and then maximize the (exact) achievable secrecy rate to update phase shifts for a given input covariance. We present a convergence proof and the associated complexity analysis of the proposed algorithm. Numerical results are provided to demonstrate the superiority of the proposed method compared to a known solution, and also to show the effect of different parameters of interest on the achievable secrecy rate of the IRS-assisted MIMOME WTC.

I. INTRODUCTION

Due to the broadcast nature of radio links, wireless communications over these channels are highly vulnerable to eavesdropping. This issue is extremely important for military applications. Many measures have been taken to mitigate such vulnerability. Among them, physical layer security (PLS) has received increasing attention as one of the promising techniques to deliver secure communication with low-complexity and possibly (cryptographic) keyless transmission. The most fundamental information-theoretic model for the study of PLS is so-called the wiretap channel (WTC), where an eavesdropper aims to decode the information intended to be exchanged between a transmitter and a legitimate receiver [1].

On the other hand, with the recent developments in the software-controlled hypersurface technology, it is now been possible to steer the radio waves falling on these hypersurfaces in a controlled fashion [2]. Therefore, in order to exploit the benefits of these hypersurfaces, termed as the intelligent reflecting surface (IRS), in the context of PLS, the problem of secrecy rate maximization (SRM) was recently considered in several works including [3]–[6]. The IRS-assisted multiple-input multiple-output multi-antenna-eavesdropper (MIMOME) WTC has been studied very recently in [3], where in order to maximize the secrecy rate of the system under consideration, the authors presented an alternating optimization (AO) algorithm in combination with minorization-maximization (MM)

algorithm. Also, in [4] the SRM problem for an IRS-assisted MIMOME WTC was studied for both with and without the knowledge of eavesdropper’s channel, where the authors proposed an AO-based algorithm. In [5], the SRM problem for IRS-assisted MIMOME WTC with both continuous as well as discrete phase shifts at the IRS was considered, where a successive convex approximation (SCA) based AO algorithm was used to find a suboptimal solution.

In this paper, we propose an efficient algorithm to find the input covariance matrix and the IRS phase shifts to maximize the achievable secrecy rate of the IRS-assisted MIMOME WTC using the block successive maximization (BSM) framework [7]. More specifically, a lower bound on the achievable secrecy rate is considered when optimizing the input covariance matrix and exact maximization is performed for each individual phase shift. In particular, these optimization steps are done using closed-form expressions. We compare the convergence speed and average run time of the proposed solution with an existing method to establish the superiority of our proposed method. Extensive numerical experiments are also carried out to demonstrate the effect of different system parameters, such as the number of reflecting elements at the IRS, the number of receive antennas at the Eavesdropper and the power transmitted from the transmitter, on the achievable secrecy rate of the considered IRS-assisted MIMOME WTC.

Notation: In this paper, we use bold uppercase and lowercase letters to denote matrices and vectors, respectively. $(\cdot)^\dagger$, $(\cdot)^T$ and $(\cdot)^*$ represent the Hermitian transpose, ordinary transpose and conjugate operators, respectively. We use $\mathbb{C}^{M \times N}$ to denote the space of $M \times N$ complex matrices. By $\mathbf{Y}_{i,j}$ we represent the j -th element of i -th row of matrix \mathbf{Y} ; $\text{diag}(\mathbf{y})$ denotes the diagonal square matrix whose (main) diagonal elements are taken from \mathbf{y} . \mathbf{I} and $\mathbf{0}$ specify identity and zero matrices respectively, the size of which can be easily inferred from the context. We denote the trace and determinant of the matrix \mathbf{Y} by $\text{tr}(\mathbf{Y})$ and $|\mathbf{Y}|$, respectively. Furthermore, we represent the expected value of a random variable by $\mathbb{E}[\cdot]$ and the real part of a complex number by $\Re\{\cdot\}$. For $\mathbf{y} \in \mathbb{R}^N$, $[\mathbf{y}]_+ = [\max(y_1, 0), \max(y_2, 0), \dots, \max(y_N, 0)]$, where \mathbb{R} denotes the set of real numbers. By $\mathbf{A} \succeq$ (resp. \succ) \mathbf{B} we mean $\mathbf{A} - \mathbf{B}$ is positive semidefinite (resp. definite). $|x|$ and $\angle x$ denote the modulus and the phase of a complex number x .

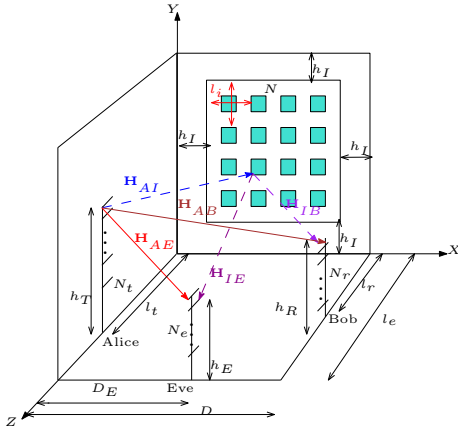


Figure 1. A block diagram of IRS-assisted MIMOME WTC system.

II. SYSTEM MODEL AND PROBLEM FORMULATION

In this section, we describe the system model and formulate the problem of maximizing the achievable secrecy rate for the system under consideration .

A. System Model

Let us consider an IRS-aided MIMOME WTC system where Alice is the transmitter, Bob is the (legitimate) receiver, and Eve is the eavesdropper. The numbers of antennas at Alice, Bob and Eve are N_t , N_r , and N_e , respectively, and the IRS is made-up of N low-cost passive reflecting elements. The system model is shown in Fig. 1. The locations of Alice, Bob and Eve in 3-dimensional Euclidean space are $(0, 0, l_t)$, $(D, 0, l_r)$ and $(D_E, 0, l_e)$, respectively. The height (measured from the X - Z plane) of the top-most antenna at Alice, Bob and Eve is respectively given by h_T , h_R , and h_E . The distance between each antenna at Alice is denoted by l_a , and that between each antenna at Bob and Eve are respectively denoted by l_b and l_e . The distance of an IRS element to its immediate neighboring one is denoted by l_i . The complex-valued channel matrices for the Alice-IRS, IRS-Bob, IRS-Eve, Alice-Bob and Alice-Eve links are denoted by $\mathbf{H}_{AI} \in \mathbb{C}^{N \times N_t}$, $\mathbf{H}_{IB} \in \mathbb{C}^{N_r \times N}$, $\mathbf{H}_{IE} \in \mathbb{C}^{N_e \times N}$, $\mathbf{H}_{AB} \in \mathbb{C}^{N_b \times N_t}$, and $\mathbf{H}_{AE} \in \mathbb{C}^{N_e \times N_t}$, respectively. It is assumed that all these channel matrices are quasi-static and perfectly known at all of the nodes.

The received signals at Bob and Eve are, respectively, expressed as

$$\begin{aligned} \mathbf{y}_b &= \mathbf{H}_{AB}\mathbf{x} + \mathbf{H}_{IB}\mathbf{Z}(\boldsymbol{\theta})\mathbf{H}_{AI}\mathbf{x} + \mathbf{n}_b, \\ \mathbf{y}_e &= \mathbf{H}_{AE}\mathbf{x} + \mathbf{H}_{IE}\mathbf{Z}(\boldsymbol{\theta})\mathbf{H}_{AI}\mathbf{x} + \mathbf{n}_e, \end{aligned} \quad (1)$$

where $\mathbf{x} \in \mathbb{C}^{N_t \times 1}$ represents the transmitted signal from Alice; $\mathbf{n}_b \sim \mathcal{CN}(\mathbf{0}, \sigma_b^2 \mathbf{I})$ and $\mathbf{n}_e \sim \mathcal{CN}(\mathbf{0}, \sigma_e^2 \mathbf{I})$ are the additive white Gaussian noise at Bob and Eve, respectively. In (1), $\mathbf{Z}(\boldsymbol{\theta}) \triangleq \text{diag}(\boldsymbol{\theta})$, where $\boldsymbol{\theta} \triangleq [\theta_1, \theta_2, \dots, \theta_N]^T \in \mathbb{C}^{N \times 1}$, $\theta_i = e^{j\phi_i}$, $i \in \mathcal{I} \triangleq \{1, 2, \dots, N\}$, and $\phi_i \in [0, 2\pi)$ denotes the phase shift induced by the i -th reflecting element at the IRS.

B. Problem Formulation

Let $\mathbf{X} \triangleq \mathbb{E}\{\mathbf{x}\mathbf{x}^\dagger\} \succeq \mathbf{0}$ be the input covariance matrix. Then for given \mathbf{X} and $\boldsymbol{\theta}$, the following secrecy rate (in nat/s/Hz)

between Alice and Bob is achievable (c.f. [8])

$$C_s(\boldsymbol{\theta}, \mathbf{X}) = [C_B(\boldsymbol{\theta}, \mathbf{X}) - C_E(\boldsymbol{\theta}, \mathbf{X})]_+, \quad (2)$$

where $C_B(\mathbf{X})$ and $C_E(\mathbf{X})$ denote the achievable rate at Bob and Eve, respectively, defined as

$$C_B(\boldsymbol{\theta}, \mathbf{X}) = \ln |\mathbf{I} + \mathbf{H}_B(\boldsymbol{\theta})\mathbf{X}\mathbf{H}_B^\dagger(\boldsymbol{\theta})| \quad (3a)$$

$$C_E(\boldsymbol{\theta}, \mathbf{X}) = \ln |\mathbf{I} + \mathbf{H}_E(\boldsymbol{\theta})\mathbf{X}\mathbf{H}_E^\dagger(\boldsymbol{\theta})| \quad (3b)$$

where $\mathbf{H}_B(\boldsymbol{\theta}) \triangleq \bar{\mathbf{H}}_{AB} + \bar{\mathbf{H}}_{IB}\mathbf{Z}(\boldsymbol{\theta})\mathbf{H}_{AI}$, $\mathbf{H}_E(\boldsymbol{\theta}) \triangleq \bar{\mathbf{H}}_{AE} + \bar{\mathbf{H}}_{IE}\mathbf{Z}(\boldsymbol{\theta})\mathbf{H}_{AI}$, $\bar{\mathbf{H}}_{AB} \triangleq \frac{1}{\sigma_b} \mathbf{H}_{AB}$, $\bar{\mathbf{H}}_{IB} \triangleq \frac{1}{\sigma_b} \mathbf{H}_{IB}$, $\bar{\mathbf{H}}_{AE} \triangleq \frac{1}{\sigma_e} \mathbf{H}_{AE}$ and $\bar{\mathbf{H}}_{IE} \triangleq \frac{1}{\sigma_e} \mathbf{H}_{IE}$.

The problem of SRM under the sum power constraint (SPC) reads

$$\begin{aligned} & \text{maximize } C_s(\boldsymbol{\theta}, \mathbf{X}) \\ & \mathbf{X} \in \mathcal{X}, \boldsymbol{\theta} \in \Theta \end{aligned} \quad (4)$$

where

$$\mathcal{X} = \{\mathbf{X} : \mathbf{X} \succeq \mathbf{0} \mid \text{tr}(\mathbf{X}) \leq P_0\}, \quad (5)$$

$$\Theta = \{\boldsymbol{\theta} : |\theta_i| = 1, \forall i \in \mathcal{I}\},$$

and P_0 is the maximum power budget at Alice. Note that in (5), $\text{tr}(\mathbf{X}) \leq P_0$ denotes the transmit power constraint and $|\theta_i| = 1$ denotes the unit-modulus constraint.

To appreciate the novelty of our proposed method presented in the next section for solving (4), we discuss the drawbacks of existing solutions known to us for solving the same problem. As mentioned previously in the introduction section, an AO-based algorithm was presented in [4] that alternately optimizes \mathbf{X} and $\boldsymbol{\theta}$ while the other variable is fixed. More specifically, a barrier method was developed to find \mathbf{X} for a given $\boldsymbol{\theta}$, and then for a given \mathbf{X} , each θ_i was found using Dinkelbach's method. Similarly, an AO-like algorithm was proposed in [9] but an SCA method was derived for finding \mathbf{X} for a given $\boldsymbol{\theta}$, and then each θ_i is optimized sequentially using a linear search procedure. It can easily be noted that both the methods mentioned above incur high complexity to produce a solution. Motivated by this, in the next section, we propose an efficient method based on the BSM to find a stationary solution to problem (4).

III. CLOSED-FORM DESIGN BASED ON BLOCK SUCCESSIVE MAXIMIZATION

A. Algorithm Description

The proposed method is based on the BSM method [7] where \mathbf{X} and each θ_i are viewed as individual blocks. We note that the main principle of the BSM is that a single block is updated in each iteration using a proper bound or exact optimization. The BSM method is particularly efficient if the optimization at each step is computationally cheap. To this end we propose an iterative method as follows:

- We sequentially update each phase shift θ_i , while other variables are fixed and *exact optimization* is considered. We derive closed-form expressions for this step, rather than using Dinkelbach's method [4] or a line search [9].
- We update \mathbf{X} using a lower bound that leads to a water-filling-like solution. This step is different from the SCA-based method in [9] where the lower bound is repeatedly solved. In contrast we only maximize the lower bound

once in each iteration. Despite this, the proposed method is provably convergent to a stationary point of (4).

The details of the proposed algorithm are given in the following subsections.

1) *Optimizing θ_i for given \mathbf{X} and other phase shifts $\theta_j, j \in \{\mathcal{I} \setminus i\}$* : The optimization of each θ_i , while remaining $\theta_j, j \in \{\mathcal{I} \setminus i\}$ and \mathbf{X} are held fixed, is formulated as

$$\underset{\theta_i}{\text{maximize}} \quad \bar{C}_s(\theta_i) \quad (6a)$$

$$\text{subject to} \quad |\theta_i| = 1, \quad (6b)$$

where

$$\bar{C}_s(\theta_i) = \ln \left| \mathbf{I} + \theta_i \mathbf{P}_i^{-1} \mathbf{Q}_i + \theta_i^* \mathbf{P}_i^{-1} \mathbf{Q}_i^\dagger \right| - \ln \left| \mathbf{I} + \theta_i \mathbf{R}_i^{-1} \mathbf{S}_i + \theta_i^* \mathbf{R}_i^{-1} \mathbf{S}_i^\dagger \right|, \quad (7)$$

and detailed expressions for \mathbf{P}_i , \mathbf{Q}_i , \mathbf{R}_i and \mathbf{S}_i are given in Appendix A. We now derive a closed-solution for (7) for the non-trivial case where $\text{tr}(\mathbf{P}_i^{-1} \mathbf{Q}_i) \neq 0$ and $\text{tr}(\mathbf{R}_i^{-1} \mathbf{S}_i) \neq 0$, and refer the interested readers to [4] for the trivial cases where $\text{tr}(\mathbf{P}_i^{-1} \mathbf{Q}_i) = 0$ and/or $\text{tr}(\mathbf{R}_i^{-1} \mathbf{S}_i) = 0$.

Let $\mathbf{P}_i^{-1} \mathbf{Q}_i = \tilde{\mathbf{U}}_{ib} \tilde{\Sigma}_{ib} \tilde{\mathbf{U}}_{ib}^\dagger$ be the eigenvalue decomposition (EVD) of $\mathbf{P}_i^{-1} \mathbf{Q}_i$. Since \mathbf{Q}_i is a rank-1 matrix we can write $\tilde{\Sigma}_{ib} = \text{diag}([\gamma_{ib}, 0, \dots, 0]^\top)$ where γ_{ib} is only non-zero eigenvalue of $\mathbf{P}_i^{-1} \mathbf{Q}_i$. Similarly, let $\tilde{\mathbf{U}}_{ie} \tilde{\Sigma}_{ie} \tilde{\mathbf{U}}_{ie}^\dagger = \mathbf{R}_i^{-1} \mathbf{S}_i$ be the EVD of $\mathbf{R}_i^{-1} \mathbf{S}_i$ where $\tilde{\Sigma}_{ie} = \text{diag}([\gamma_{ie}, 0, \dots, 0]^\top)$ and γ_{ie} is only non-zero eigenvalue of $\mathbf{R}_i^{-1} \mathbf{S}_i$. Furthermore, let $\mathbf{A}_i = \tilde{\mathbf{U}}_{ib}^\dagger \mathbf{P}_i \tilde{\mathbf{U}}_{ib}$, and $\tilde{\mathbf{a}}_i$ denotes the first column of \mathbf{A}_i^{-1} , and $\tilde{\mathbf{a}}_i^\top$ denotes the first row of \mathbf{A}_i . Similarly, we define $\mathbf{B}_i = \tilde{\mathbf{U}}_{ie}^\dagger \mathbf{R}_i \tilde{\mathbf{U}}_{ie}$, and $\tilde{\mathbf{b}}_i$ denotes the first column of \mathbf{B}_i^{-1} , and $\tilde{\mathbf{b}}_i^\top$ denotes the first row of \mathbf{B}_i . We can further rewrite (7) as (c.f. [10])

$$\bar{C}_s(\theta_i) = \ln \left(\frac{2\Re(\gamma_{ib}\theta_i) + \delta_{ib}}{2\Re(\gamma_{ie}\theta_i) + \delta_{ie}} \right), \quad (8)$$

where $\delta_{ib} = 1 + |\gamma_{ib}|^2(1 - \tilde{a}_{i1}\tilde{a}_{i1}^*)$, $\delta_{ie} = 1 + |\gamma_{ie}|^2(1 - \tilde{b}_{i1}\tilde{b}_{i1}^*)$, and \tilde{a}_{i1} and \tilde{a}_{i1}^* denote the first element of $\tilde{\mathbf{a}}_i$ and $\tilde{\mathbf{a}}_i^\top$, respectively. It is easy to see that using (8), problem (6) is equivalent to

$$\underset{\theta_i}{\text{maximize}} \quad \frac{2\Re(\gamma_{ib}\theta_i) + \delta_{ib}}{2\Re(\gamma_{ie}\theta_i) + \delta_{ie}} \quad (9a)$$

$$\text{subject to} \quad |\theta_i| = 1. \quad (9b)$$

Let $\phi_{ib} = \angle \gamma_{ib}$, $\phi_{ie} = \angle \gamma_{ie}$ and $\lambda_{ib} = 2|\gamma_{ib}|$ and $\lambda_{ie} = 2|\gamma_{ie}|$. Then (9) is equivalent to

$$\underset{\phi_i}{\text{maximize}} \quad \frac{\lambda_{ib} \cos(\phi_i - \phi_{ib}) + \delta_{ib}}{\lambda_{ie} \cos(\phi_i - \phi_{ie}) + \delta_{ie}} = f(\phi_i) \quad (10a)$$

$$\text{subject to} \quad 0 \leq \phi_i < 2\pi. \quad (10b)$$

The derivative of the objective function in (10) is given by

$$f'(\phi_i) = \frac{\lambda_{ib}\lambda_{ie} \sin(\phi_{ib} - \phi_{ie}) - \lambda_i \sin(\phi_i - \psi_i)}{(\lambda_{ie} \cos(\phi_i - \phi_{ie}) + \delta_{ie})^2}, \quad (11)$$

where

$$\lambda_i \triangleq \sqrt{\lambda_{ib}^2 \delta_{ie}^2 + \lambda_{ie}^2 \delta_{ib}^2 - 2\lambda_{ib}\lambda_{ie}\delta_{ib}\delta_{ie} \cos(\phi_{ib} - \phi_{ie})}, \quad (12)$$

$$\psi_i \triangleq \arctan \left\{ \frac{-\lambda_{ib}\delta_{ie} \sin(\phi_{ib}) + \lambda_{ie}\delta_{ib} \sin(\phi_{ie})}{\lambda_{ib}\delta_{ie} \cos(\phi_{ib}) - \lambda_{ie}\delta_{ib} \cos(\phi_{ie})} \right\}. \quad (13)$$

We note that $\delta_{iu} \geq 1 + \lambda_{iu}$ for $u \in \{b, e\}$, which holds due to their definitions. Thus, the equation $f'(\phi_i) = 0$ has two

possible solutions as follows:

$$\phi_{i_1} = \arcsin \left\{ \frac{\lambda_{ib}\lambda_{ie}}{\lambda_i} \sin(\phi_{ib} - \phi_{ie}) \right\} + \psi_i, \quad (14)$$

$$\phi_{i_2} = \pi - \arcsin \left\{ \frac{\lambda_{ib}\lambda_{ie}}{\lambda_i} \sin(\phi_{ib} - \phi_{ie}) \right\} + \psi_i. \quad (15)$$

Thus, the optimal solution to (6) is found as

$$\theta_i^* = e^{j\phi_i^*} \quad (16)$$

where¹

$$\phi_i^* = \arg \max \{f(0), f(\phi_{i_1}), f(\phi_{i_2})\}. \quad (17)$$

Algorithm 1: Block Successive Maximization Method

Input: $\mathbf{X}_0 \in \mathcal{X}$, $\boldsymbol{\theta}_0 \in \Theta$

Output: $\mathbf{X}_k \in \mathcal{X}$, $\boldsymbol{\theta}_k \in \Theta$

1 $k \leftarrow 1$;

2 **repeat**

3 **for** $i \in \mathcal{I}$ **do**

4 Compute θ_i according to (16) for fixed \mathbf{X}_{k-1}

5 $\theta_i \leftarrow \theta_i^*$

6 **end**

7 Find \mathbf{X}_k for fixed $\boldsymbol{\theta}_k$ according to (19)

8 $k \leftarrow k + 1$

9 **until** convergence;

2) *Optimizing \mathbf{X} for given $\boldsymbol{\theta}$* : The next step is to optimize \mathbf{X} for a given $\boldsymbol{\theta}$. Instead of maximizing the secrecy rate exactly, we consider a lower bound in this step. Let \mathbf{X}_{k-1} be the value of \mathbf{X} at iteration $k - 1$. Then, due to the concavity of the term $\ln |\cdot|$ it follows that

$$C(\boldsymbol{\theta}_k, \mathbf{X}) \leq \hat{C}_s(\boldsymbol{\theta}_k, \mathbf{X}) = \ln |\mathbf{I} + \mathbf{H}_B(\boldsymbol{\theta}_k) \mathbf{X} \mathbf{H}_B^\dagger(\boldsymbol{\theta}_k)| - \ln |\mathbf{I} + \mathbf{H}_E(\boldsymbol{\theta}_k) \mathbf{X}_{k-1} \mathbf{H}_E^\dagger(\boldsymbol{\theta}_k)| - \text{tr}((\boldsymbol{\Phi}_{k-1})(\mathbf{X} - \mathbf{X}_{k-1})), \quad (18)$$

where $\boldsymbol{\Phi}_{k-1} = \mathbf{H}_E^\dagger(\boldsymbol{\theta})(\mathbf{I} + \mathbf{H}_E(\boldsymbol{\theta}) \mathbf{X}_{k-1} \mathbf{H}_E^\dagger(\boldsymbol{\theta}))^{-1} \mathbf{H}_E(\boldsymbol{\theta})$. Note that (18) is obtained by using a first-order approximation of the term $\ln |\mathbf{I} + \mathbf{H}_E(\boldsymbol{\theta}) \mathbf{X} \mathbf{H}_E^\dagger(\boldsymbol{\theta})|$ around \mathbf{X}_{k-1} . Next, we update \mathbf{X}_k as $\mathbf{X}_k = \arg \max \{\hat{C}_s(\boldsymbol{\theta}_k, \mathbf{X}) \mid \mathbf{X} \in \mathcal{X}\}$ which is equivalent to

$$\underset{\mathbf{X} \geq \mathbf{0}}{\text{maximize}} \quad \ln |\mathbf{I} + \mathbf{H}_B(\boldsymbol{\theta}) \mathbf{X} \mathbf{H}_B^\dagger(\boldsymbol{\theta})| - \text{tr}(\boldsymbol{\Phi}_{k-1} \mathbf{X}) \quad (19a)$$

$$\text{subject to} \quad \text{tr}(\mathbf{X}) \leq P_0. \quad (19b)$$

The aforementioned problem (19) admits a *water-filling solution* [11]. To lighten the notations we write \mathbf{H}_B instead of $\mathbf{H}_B(\boldsymbol{\theta})$. Let $\mu \geq 0$ be the Lagrangian multiplier of (19b). Then the *partial* Lagrangian multiplier of (19) is

$$\mathcal{L}(\mathbf{X}, \mu) = \ln |\mathbf{I} + \mathbf{H}_B \mathbf{X} \mathbf{H}_B^\dagger| - \text{tr}(\boldsymbol{\Phi}_{k-1} \mathbf{X}) - \mu(\text{tr}(\mathbf{X}) - P_0) = \ln |\mathbf{I} + \mathbf{H}_B \mathbf{X} \mathbf{H}_B^\dagger| - \text{tr}(\bar{\boldsymbol{\Phi}}_{k-1} \mathbf{X}) + \mu P_0. \quad (20)$$

where $\bar{\boldsymbol{\Phi}}_{k-1} = \boldsymbol{\Phi}_{k-1} + \mu \mathbf{I}$. The dual function is given by

$$g(\mu) = \max_{\mathbf{X} \geq \mathbf{0}} \ln |\mathbf{I} + \mathbf{H}_B \mathbf{X} \mathbf{H}_B^\dagger| - \text{tr}(\bar{\boldsymbol{\Phi}}_{k-1} \mathbf{X}) + \mu P_0. \quad (21)$$

¹We can also check the second derivative of these three critical points to find the optimal solution but comparing their objective values is much simpler.

To evaluate the dual function for a given μ , let $\bar{\mathbf{X}} \triangleq \bar{\Phi}_{k-1}^{1/2} \mathbf{X} \bar{\Phi}_{k-1}^{1/2}$. Then the above maximization is equivalent to $\max_{\mathbf{X} \succeq \mathbf{0}} \mathcal{L}(\bar{\mathbf{X}}, \mu) = \ln |\mathbf{I} + \mathbf{H}_B \bar{\Phi}_{k-1}^{-1/2} \bar{\mathbf{X}} \bar{\Phi}_{k-1}^{-1/2} \mathbf{H}_B^\dagger| - \text{tr}(\bar{\mathbf{X}})$. (22)

Denote the eigenvalue decomposition (EVD) of $\bar{\Phi}_{k-1}^{-1/2} \mathbf{H}_B^\dagger \mathbf{H}_B \bar{\Phi}_{k-1}^{-1/2}$ by $\mathbf{U} \Sigma \mathbf{U}^\dagger$ where $\mathbf{U} \in \mathbb{C}^{N_t \times N_t}$ is unitary, $\Sigma = \text{diag}(\sigma_1, \sigma_2, \dots, \sigma_r, 0, \dots, 0)$, and r is the rank of $\bar{\Phi}_{k-1}^{-1/2} \mathbf{H}_B$ and let $\dot{\mathbf{X}} = \mathbf{U}^\dagger \bar{\mathbf{X}} \mathbf{U}$. Then (22) is further equivalent to

$$\max_{\dot{\mathbf{X}} \succeq \mathbf{0}} \mathcal{L}(\dot{\mathbf{X}}, \mu) = \ln |\mathbf{I} + \Sigma \dot{\mathbf{X}}| - \text{tr}(\dot{\mathbf{X}}). \quad (23)$$

It is now easy to see that we can assume $\dot{\mathbf{X}}$ to be diagonal (due to Hadamard's inequality), and the optimal solution to (23) is given by $\dot{\mathbf{X}} = \text{diag}([1 - \frac{1}{\sigma_1}]_+, \dots, [1 - \frac{1}{\sigma_r}]_+, 0, \dots, 0)$. In summary, the optimal solution to (21) is

$$\mathbf{X} = \bar{\Phi}_{k-1}^{-1/2} \mathbf{U} \dot{\mathbf{X}} \mathbf{U}^\dagger \bar{\Phi}_{k-1}^{-1/2}. \quad (24)$$

The next step is to solve the dual problem $\min \{g(\mu) \mid \mu \geq 0\}$ which can be done efficiently using a bisection search. We refer the interested readers to [11] for further details.

The overall algorithm to solve (4) is summarized in Algorithm 1.

B. Convergence Analysis

We now show that Algorithm 1 indeed converges to a stationary point of (4). In particular the following lemma is in order

Lemma 1. *The objective sequence generated by Algorithm 1 is monotonically increasing, i.e.,*

$$C_s(\boldsymbol{\theta}_k, \mathbf{X}_k) \geq C_s(\boldsymbol{\theta}_k, \mathbf{X}_{k-1}) \geq C_s(\boldsymbol{\theta}_{k-1}, \mathbf{X}_{k-1}). \quad (25)$$

Also, the iterate sequence $(\boldsymbol{\theta}_k, \mathbf{X}_k)$ converges to a limit point which is a stationary solution of (4).

Proof: See Appendix B. ■

C. Complexity Analysis

In this subsection we provide the complexity analysis of Algorithm 1. In particular we adopt the big- \mathcal{O} notation and present the number of complex multiplications for each iteration of Algorithm 1. To compute \mathbf{P}_i we use (27a) and note that \mathbf{P} only needs to be computed once for all \mathbf{P}_i . The complexity to obtain \mathbf{P} is $\mathcal{O}(NN_r^2)$ and to compute each \mathbf{P}_i we require $\mathcal{O}(N_t^2 N_r)$ additional complex multiplications. In the same way, the complexity to compute each \mathbf{R}_i is $\mathcal{O}(N_t^2 N_e)$. We skip the complexity of obtaining \mathbf{Q}_i and \mathbf{S}_i since it is much less than that of obtaining \mathbf{P}_i and \mathbf{R}_i . It is easy to see that the complexity of computing $\mathbf{P}_i^{-1} \mathbf{Q}_i$ and its EVD is $\mathcal{O}(N_r^3)$. Similarly, the complexity of computing $\mathbf{R}_i^{-1} \mathbf{S}_i$ and its EVD is $\mathcal{O}(N_e^3)$. The complexity of computing \tilde{a}_{i1} , \tilde{a}_{i1} , \tilde{b}_{i1} , and \tilde{b}_{i1} , the closed-form expressions for each optimal θ_i^* is much less than that of computing other terms, and thus is omitted. When $\boldsymbol{\theta}$ is fixed, it can be shown that the complexity for solving (19a) is $\mathcal{O}(N_e^3 + N_t^2 N_e + N_t N_e^2 + N_t^3)$. In summary, the per-iteration complexity of Algorithm 1 is $\mathcal{O}(N(N_r^2 + N_t^2 N_r + N_t^2 N_e + N_r^3 + N_e^3) + N_t N_e^2 + N_t^3)$.

IV. NUMERICAL ANALYSIS

In this section, we describe the channel modeling, and present numerical results and discussions.

A. Channel Modeling

We consider the scenario where the small-scale fading for all of the wireless links are assumed to follow Rician distribution. Therefore, Alice-Bob and Alice-Eve links are respectively modeled as [12], $\mathbf{H}_{AB} = \sqrt{\frac{\zeta_{AB}^{-1}}{\kappa+1}} (\sqrt{\kappa} \mathbf{H}_{AB, \text{LOS}} + \mathbf{H}_{AB, \text{NLOS}})$ and $\mathbf{H}_{AE} = \sqrt{\frac{\zeta_{AE}^{-1}}{\kappa+1}} (\sqrt{\kappa} \mathbf{H}_{AE, \text{LOS}} + \mathbf{H}_{AE, \text{NLOS}})$, where $\mathbf{H}_{AB, \text{LOS}}, \mathbf{H}_{AB, \text{NLOS}} \in \mathbb{C}^{N_r \times N_t}$, and $\mathbf{H}_{AE, \text{LOS}}, \mathbf{H}_{AE, \text{NLOS}} \in \mathbb{C}^{N_e \times N_t}$. Here $\mathbf{H}_{AB, \text{LOS}}$ accounts for the line-of-sight (LOS) components between Alice to Bob, and the elements in $\mathbf{H}_{AB, \text{LOS}}$ are defined as $e^{-j2\pi l_{r,t}/v}$ where $l_{r,t}$ is the distance between the t -th antenna of Alice and the r -th antenna of Bob, and v denotes wavelength of the transmitted signal. Moreover, $\kappa = 1$ denotes the Rician K factor, and $\mathbf{H}_{AB, \text{NLOS}} \sim \mathcal{CN}(\mathbf{0}, \mathbf{I})$ accounts for the non-line-of-sight (NLOS) components between Alice and Bob. Similarly, $\mathbf{H}_{AE, \text{LOS}}$ accounts for the LOS components between Alice and Eve, and the elements in $\mathbf{H}_{AE, \text{LOS}}$ are defined as $e^{-j2\pi l_{e,t}/v}$ where $l_{e,t}$ is the distance between the t -th antenna of Alice and the e -th antenna of Eve, and $\mathbf{H}_{AE, \text{NLOS}} \sim \mathcal{CN}(\mathbf{0}, \mathbf{I})$ accounts for the NLOS components between Alice and Eve. In this paper, we consider $v = 15$ cm, which corresponds to the carrier frequency of 2 GHz. We note that $l_{r,t}$ and $l_{e,t}$ are calculated according to the system model in Fig. 1. Moreover, ζ_{AB} and ζ_{AE} denote the free-space path loss (FSPL) coefficients, defined as $\zeta_{AB} \triangleq (4\pi/v)^2 l_{AB}^\varepsilon$ and $\zeta_{AE} \triangleq (4\pi/v)^2 l_{AE}^\varepsilon$, respectively [13]. We define $l_{AB} \triangleq \sqrt{D^2 + (l_t - l_r)^2}$ as the distance between Alice and Bob (i.e., the distance between $(0, 0, l_t)$ and $(D, 0, l_r)$), $l_{AE} \triangleq \sqrt{D_E^2 + (l_t - l_e)^2}$ as the distance between Alice and Eve (i.e., the distance between $(0, 0, l_t)$ and $(D_E, 0, l_e)$), and $\varepsilon = 3$ is the path loss exponent.

In a similar fashion, the channel between Alice and IRS, and that between IRS and Bob are modeled as $\mathbf{H}_{AI} = \sqrt{\frac{1}{\kappa+1}} (\sqrt{\kappa} \mathbf{H}_{AI, \text{LOS}} + \mathbf{H}_{AI, \text{NLOS}})$ and $\mathbf{H}_{IB} = \sqrt{\frac{\zeta_{IB}^{-1}}{\kappa+1}} (\sqrt{\kappa} \mathbf{H}_{IB, \text{LOS}} + \mathbf{H}_{IB, \text{NLOS}})$, respectively, where $\mathbf{H}_{AI, \text{LOS}}, \mathbf{H}_{AI, \text{NLOS}} \in \mathbb{C}^{N \times N_t}$, and $\mathbf{H}_{IB, \text{LOS}}, \mathbf{H}_{IB, \text{NLOS}} \in \mathbb{C}^{N_r \times N}$. The elements in $\mathbf{H}_{AI, \text{LOS}}$ are defined as $e^{-j2\pi l_{i,t}/v}$ with $l_{i,t}$ being the distance between the t -th transmit antenna of Alice and the i -th reflecting plate of IRS, and $\mathbf{H}_{AI, \text{NLOS}} \sim \mathcal{CN}(\mathbf{0}, \mathbf{I})$. Analogously, the elements in $\mathbf{H}_{IB, \text{LOS}}$ are defined as $e^{-j2\pi l_{r,i}/v}$ with $l_{r,i}$ denoting the distance between the r -th receiver antenna of Bob and the i -th reflecting element of the IRS and $\mathbf{H}_{IB, \text{NLOS}} \sim \mathcal{CN}(\mathbf{0}, \mathbf{I})$. The FSPL coefficient ζ_{IB} is modeled as (c.f. [14]) $\zeta_{IB} = \frac{256\pi^2 v^{-4} D_t^2 D_r^2}{((l_t/D_t) + (l_r/D_r))^2}$, where $D_t \triangleq \sqrt{(D/2)^2 + l_t^2}$ and $D_r \triangleq \sqrt{(D/2)^2 + l_r^2}$. Following a similar line of arguments, the channel between IRS and Eve is modeled as $\mathbf{H}_{IE} = \sqrt{\frac{\zeta_{IE}^{-1}}{\kappa+1}} (\sqrt{\kappa} \mathbf{H}_{IE, \text{LOS}} + \mathbf{H}_{IE, \text{NLOS}})$, where $\mathbf{H}_{IE, \text{LOS}}, \mathbf{H}_{IE, \text{NLOS}} \in \mathbb{C}^{N_e \times N}$. The elements in $\mathbf{H}_{IE, \text{LOS}}$

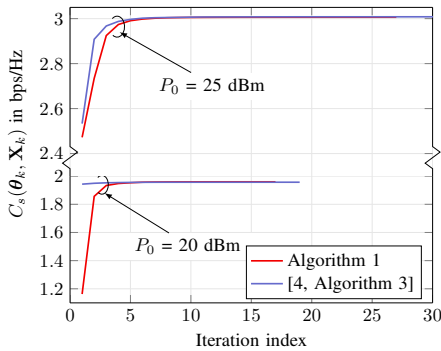


Figure 2. Convergence comparison for $(N_t, N_r, N_e, N) = (4, 3, 2, 25)$.

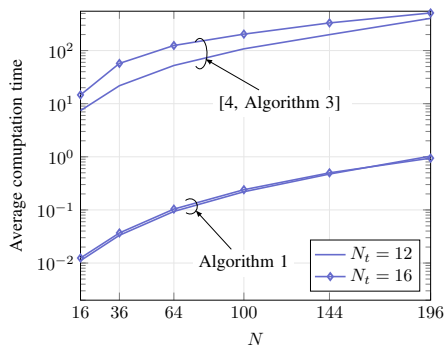


Figure 3. Average computation time for various algorithms for $(N_r, N_e) = (8, 6)$ and $P_0 = 10$ dB.

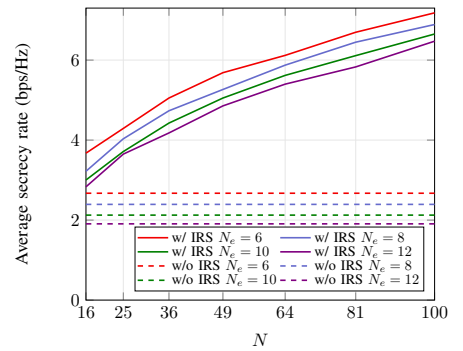


Figure 4. The average secrecy rate with $(N_t, N_r) = (12, 8)$ and $P_0 = 25$ dBm.

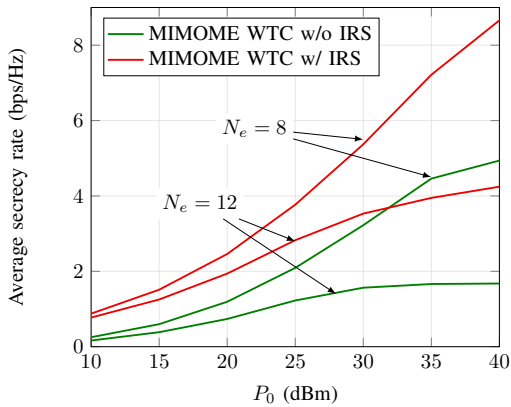


Figure 5. Comparison of the secrecy rate for MIMOME WTC and IRS-assisted MIMOME WTC for $(N_t, N_r, N) = (8, 6, 25)$.

are defined as $e^{-j2\pi l_{e,i}/v}$ with $l_{e,i}$ being the distance between the e -th eavesdrop antenna and i -th reflecting plate of IRS, and $\mathbf{H}_{JE, NLOS} \sim \mathcal{CN}(\mathbf{0}, \mathbf{I})$. Moreover, the FSPL coefficient for IRS-Eve links is expressed as $\zeta_{IE} = \frac{256\pi^2 v^{-4} \mathcal{D}_t^2 \mathcal{D}_e^2}{\left((l_t/\mathcal{D}_t) + (l_e/\sqrt{\mathcal{D}_E + l_e^2}) \right)^2}$, where $\mathcal{D}_e \triangleq \sqrt{(\mathcal{D}_E/2)^2 + l_e^2}$.

B. Numerical Results

In this subsection, we provide numerical results to evaluate the performance of Algorithm 1, as well as to show the effect of different parameters of interest on the achieved secrecy rate of the IRS-assisted MIMOME system under consideration. The numerical experiments are performed using MATLAB (R2109a) on a 64-bit Windows machine with 16 GB RAM and an Intel Core i7 3.20 GHz processor. Moreover, for all the figures, we assume $\sigma_n^2 = -95$ dBW, $h_T = 3$ m, $h_R = 2.5$ m, $h_E = 2$ m, $h_I = 5$ m, $l_t = 20$ m, $l_r = 15$ m, $l_e = 35$ m, $\iota_a = 0.05$ m, $\iota_b = 0.25$ m, $\iota_e = 0.03$ m, $l_i = 0.03$ m, $D = 50$ m and $\mathcal{D}_e = 40$ m. We also assumed that all of the reflecting element at the IRS to be a square of size 0.01 m \times 0.01 m, and the gap between each reflecting element to be 0.01 m.

In Fig. 2, we show the convergence performance of Algorithm 1 for one set of randomly generated channels. We also plot the convergence of [4, Algorithm 3] for comparison. It can be noted from the figure that our BSM-based proposed method

requires a comparable number of iterations to converge, compared to the algorithm used in [4]. In particular, [4, Algorithm 3] can achieve higher secrecy rates for some initial iterations which is explained by the fact that the optimization of \mathbf{X} is done exactly, while Algorithm 1 only optimizes a lower bound of the secrecy rate. However, both methods achieves the same secrecy rate at the convergence.

The main benefit of Algorithm 1 is closed-form designs in each iteration, which eventually lead to much lower run-time to compute a solution. This point is clearly demonstrated in Fig. 3 where we compare the average run time of Algorithm 1 and [4, Algorithm 3]. It is clearly evident from the figure that our closed-form-based proposed algorithm to find a stationary solution to the secrecy maximization problem under consideration requires significantly less time compared to the existing benchmark solution, which establishes the superiority of our proposed solution.

In Fig. 4, we show the effect of increasing the number of reflecting elements, i.e., N , on the average secrecy rate of the system for different number of antennas at Eve, i.e., N_e . The average secrecy rates are obtained for 10^3 channel realizations. The benefit of using the IRS is clearly evident from the figure, as the system with IRS achieves a notably higher average secrecy rate compared to the ones without any IRS. It can also be observed from the figure that for a fixed value of N , the secrecy rate of the system reduces when the number of antennas at Eve increases since the secure degree-of-freedom for Bob decreases accordingly. However, for a fixed value of N_e , an increase in the value of N results in a significant increase in the secrecy rate of the system. This occurs because when the number of reflecting plates at IRS is large, the IRS can perform highly-focused passive beamforming towards Bob to enhance the secrecy performance of the system.

In Fig. 5, we compare the average achievable secrecy rate of the IRS-assisted MIMOME WTC system with that of the ones without IRS, for different values of the transmit power from Alice. According to [1], as $P_0 \rightarrow \infty$, the slope of the average secrecy rate approaches zero if $\text{rank}(\mathbf{H}_E(\boldsymbol{\theta})) = N_t$, and thus

¹We thank the authors of [4] for sharing the source code for their barrier method

the average secrecy rate is expected to saturate. The purpose of this numerical experiment is to understand how the IRS can improve this saturation point. We remark that $\text{rank}(\mathbf{H}_E(\boldsymbol{\theta})) = N_t$ for both the cases considered in Fig. 5, i.e., $N_e = 8$ and $N_e = 12$. It can be observed clearly from Fig. 5 that beyond a certain value of P_0 , the slope of the average secrecy rate starts decreasing, which will eventually lead to a saturation in the achieved secrecy rate for large enough values of P_0 . The important observation is that the saturated value for an IRS-assisted system is significantly larger than that of the system without IRS, which clearly establishes the superiority of the IRS-assisted systems even in the large transmit power regimes.

V. CONCLUSION

In this paper, we have proposed an efficient numerical method to maximize the achievable secrecy rate for an IRS-assisted Gaussian MIMOME WTC system. We have used a block successive maximization method to jointly optimize the transmit covariance matrix and the IRS phase shifts. The obtained results have confirmed a faster convergence and lower complexity of the proposed method compared to an existing solution which uses a combination of barrier method and bisection search. Furthermore, our results have also demonstrated the superiority of IRS-assisted systems over those without IRS, including a significantly higher achievable secrecy rate of the former in the high transmit power regime.

APPENDIX A

EXPRESSIONS FOR \mathbf{P}_i , \mathbf{Q}_i , \mathbf{R}_i , AND \mathbf{S}_i IN (7)

To obtain the expressions for \mathbf{P}_i , \mathbf{Q}_i , \mathbf{R}_i , and \mathbf{S}_i in (7) we simply group the involved matrices properly. Specifically, let $\hat{\mathbf{H}}_{AB} = \bar{\mathbf{H}}_{AB}\mathbf{X}^{1/2}$, $\hat{\mathbf{H}}_{AE} = \bar{\mathbf{H}}_{AE}\mathbf{X}^{1/2}$, and $\hat{\mathbf{H}}_{AI} = \mathbf{H}_{AI}\mathbf{X}^{1/2}$. Then, following [10], we can write \mathbf{P}_i , \mathbf{Q}_i , \mathbf{R}_i and \mathbf{S}_i , respectively, as

$$\mathbf{P}_i = \mathbf{I} + \left(\hat{\mathbf{H}}_{AB} + \sum_{j \in \{\mathcal{I} \setminus i\}} \theta_j \bar{\mathbf{h}}_j \hat{\mathbf{h}}_j^\dagger \right) \times \left(\hat{\mathbf{H}}_{AB} + \sum_{j \in \{\mathcal{I} \setminus i\}} \theta_j \bar{\mathbf{h}}_j \hat{\mathbf{h}}_j^\dagger \right)^\dagger + \bar{\mathbf{h}}_i \hat{\mathbf{h}}_i^\dagger \bar{\mathbf{h}}_i \bar{\mathbf{h}}_i^\dagger, \quad (26a)$$

$$\mathbf{Q}_i = \bar{\mathbf{h}}_i \hat{\mathbf{h}}_i^\dagger \left(\hat{\mathbf{H}}_{AB} + \sum_{j \in \{\mathcal{I} \setminus i\}} \theta_j^* \bar{\mathbf{h}}_j \hat{\mathbf{h}}_j^\dagger \right), \quad (26b)$$

$$\mathbf{R}_i = \mathbf{I} + \left(\hat{\mathbf{H}}_{AE} + \sum_{j \in \{\mathcal{I} \setminus i\}} \theta_j \tilde{\mathbf{h}}_j \hat{\mathbf{h}}_j^\dagger \right) \times \left(\hat{\mathbf{H}}_{AE} + \sum_{j \in \{\mathcal{I} \setminus i\}} \theta_j \tilde{\mathbf{h}}_j \hat{\mathbf{h}}_j^\dagger \right)^\dagger + \tilde{\mathbf{h}}_i \hat{\mathbf{h}}_i^\dagger \tilde{\mathbf{h}}_i \tilde{\mathbf{h}}_i^\dagger, \quad (26c)$$

$$\mathbf{S}_i = \tilde{\mathbf{h}}_i \hat{\mathbf{h}}_i^\dagger \left(\hat{\mathbf{H}}_{AE} + \sum_{j \in \{\mathcal{I} \setminus i\}} \theta_j^* \tilde{\mathbf{h}}_j \hat{\mathbf{h}}_j^\dagger \right), \quad (26d)$$

where $\hat{\mathbf{h}}_i$, $\bar{\mathbf{h}}_i$ and $\tilde{\mathbf{h}}_i$ are the i -th column of $\hat{\mathbf{H}}_{AI}^\dagger$, \mathbf{H}_{IB} and \mathbf{H}_{IE} , respectively. Note that we can equivalently rewrite \mathbf{P}_i and \mathbf{Q}_i as

$$\mathbf{P}_i = \mathbf{I} + (\mathbf{P} - \theta_i \bar{\mathbf{h}}_i \hat{\mathbf{h}}_i^\dagger) (\mathbf{P}^\dagger - \theta_i^* \hat{\mathbf{h}}_i \bar{\mathbf{h}}_i^\dagger) + \bar{\mathbf{h}}_i \hat{\mathbf{h}}_i^\dagger \bar{\mathbf{h}}_i \bar{\mathbf{h}}_i^\dagger \quad (27a)$$

$$\mathbf{Q}_i = \bar{\mathbf{h}}_i \hat{\mathbf{h}}_i^\dagger (\mathbf{P}^\dagger - \theta_i^* \hat{\mathbf{h}}_i \bar{\mathbf{h}}_i^\dagger), \quad (27b)$$

where $\mathbf{P} = \hat{\mathbf{H}}_{AB} + \sum_{j \in \{\mathcal{I}\}} \theta_j \bar{\mathbf{h}}_j \hat{\mathbf{h}}_j^\dagger$.

APPENDIX B

PROOF OF LEMMA 1

First, from Line 7 of Algorithm 1 we have

$$\begin{aligned} C_s(\boldsymbol{\theta}_k, \mathbf{X}_k) &\geq \hat{C}_s(\boldsymbol{\theta}_k, \mathbf{X}_k) \\ &\geq \hat{C}_s(\boldsymbol{\theta}_k, \mathbf{X}_{k-1}) = C_s(\boldsymbol{\theta}_k, \mathbf{X}_{k-1}). \end{aligned} \quad (28)$$

Note that the first inequality is due to the fact that $\hat{C}_s(\boldsymbol{\theta}_k, \mathbf{X}_k)$ is a lower bound on the secrecy rate, the second inequality is because $\mathbf{X}_k = \text{argmax}_{\mathbf{X} \in \mathcal{X}} \hat{C}_s(\boldsymbol{\theta}_k, \mathbf{X})$ and the optimal objective is no less than the objective at a feasible point, and the equality is obvious from (18). Let $\boldsymbol{\theta}_k \triangleq [\theta_{k,1}, \theta_{k,2}, \dots, \theta_{k,N}]^\top$, then Line 4 of Algorithm 1 implies the following sequence of inequalities.

$$\begin{aligned} C_s(\boldsymbol{\theta}_k, \mathbf{X}_{k-1}) &= C_s([\theta_{k,1}, \theta_{k,2}, \dots, \theta_{k,N}]^\top, \mathbf{X}_{k-1}) \\ &\geq C_s([\theta_{k,1}, \theta_{k,2}, \dots, \theta_{k,N-1}, \theta_{k-1,N}]^\top, \mathbf{X}_{k-1}) \\ &\geq C_s([\theta_{k,1}, \theta_{k,2}, \dots, \theta_{k-1,N-1}, \theta_{k-1,N}]^\top, \mathbf{X}_{k-1}) \\ &\geq C_s([\theta_{k-1,1}, \theta_{k-1,2}, \dots, \theta_{k-1,N-1}, \theta_{k-1,N}]^\top, \mathbf{X}_{k-1}) \\ &= C_s(\boldsymbol{\theta}_{k-1}, \mathbf{X}_{k-1}). \end{aligned} \quad (29)$$

Therefore, combining (28) and (29), we achieve (25).

The second part of Lemma 1 can be proved as follows. Note the the objective is bounded from above due to the power constraint. Due to (25), the objective sequence is convergent. i.e. $\lim_{k \rightarrow \infty} C_s(\boldsymbol{\theta}_k, \mathbf{X}_k) = C_s(\boldsymbol{\theta}_*, \mathbf{X}_*)$. Since the feasible set is compact, there exists a subsequence $(\boldsymbol{\theta}_{k_j}, \mathbf{X}_{k_j})$ converging to $(\boldsymbol{\theta}_*, \mathbf{X}_*)$. The proof that $(\boldsymbol{\theta}_*, \mathbf{X}_*)$ is a stationary point of (4) follows the arguments in [7], which are skipped here the the sake of brevity.

REFERENCES

- [1] A. Khisti and G. W. Wornell, "Secure transmission with multiple antennas part II: The MIMOME wiretap channel," *IEEE Trans. Inf. Theory*, vol. 56, no. 11, pp. 5515–5532, Oct. 2010.
- [2] C. Liaskos, S. Nie, A. Tsioliaridou, A. Pitsillides, S. Ioannidis, and I. Akyildiz, "A new wireless communication paradigm through software-controlled metasurfaces," *IEEE Commun. Mag.*, vol. 56, no. 9, pp. 162–169, 2018.
- [3] L. Dong and H.-M. Wang, "Secure MIMO transmission via intelligent reflecting surface," *IEEE Wireless Commun. Lett.*, vol. 9, no. 6, pp. 787–790, Jun. 2020.
- [4] —, "Enhancing secure MIMO transmission via intelligent reflecting surface," *IEEE Trans. Wireless Commun.*, vol. 19, no. 11, pp. 7543–7556, Nov. 2020.
- [5] W. Jiang, Y. Zhang, J. Wu, W. Feng, and Y. Jin, "Intelligent reflecting surface assisted secure wireless communications with multiple-transmit and multiple-receive antennas," *IEEE Access*, vol. 8, pp. 86 659–86 673, May 2020.
- [6] Z. Chu, W. Hao, P. Xiao, D. Mi, Z. Liu, M. Khalily, J. R. Kelly, and A. P. Feresidis, "Secrecy rate optimization for intelligent reflecting surface assisted MIMO system," *IEEE Trans. Inf. Forensics Security*, vol. 16, pp. 1655–1669, Jan. 2021.
- [7] M. Razaviyayn, M. Hong, and Z.-Q. Luo, "A unified convergence analysis of block successive minimization methods for nonsmooth optimization," *SIAM J. Optim.*, vol. 23, no. 2, pp. 1126–1153, 2013.
- [8] F. Oggier and B. Hassibi, "The secrecy capacity of the MIMO wiretap channel," *IEEE Trans. Inf. Theory*, vol. 57, no. 8, pp. 4961–4972, Aug. 2011.
- [9] W. Jiang, Y. Zhang, J. Wu, W. Feng, and Y. Jin, "Intelligent reflecting surface assisted secure wireless communications with multiple-transmit and multiple-receive antennas," *IEEE Access*, vol. 8, pp. 86 659–86 673, May 2020.
- [10] S. Zhang and R. Zhang, "Capacity characterization for intelligent reflecting surface aided MIMO communication," *IEEE J. Sel. Areas Commun.*, vol. 38, no. 8, pp. 1823–1838, 2020.
- [11] T. V. Nguyen, Q.-D. Vu, M. Juntti, and L.-N. Tran, "A low-complexity algorithm for achieving secrecy capacity in MIMO wiretap channels," in *Proc. IEEE ICC 2020*, Jun. 2020.
- [12] N. S. Perovic, L.-N. Tran, M. Di Renzo, and M. Flanagan, "Achievable rate optimization for MIMO systems with reconfigurable intelligent surfaces," *IEEE Trans. Wireless Commun.*, vol. 20, no. 6, pp. 3865–3882, 2021.
- [13] T. S. Rappaport, Y. Xing, G. R. MacCartney, A. F. Molisch, E. Mellios, and J. Zhang, "Overview of millimeter wave communications for fifth-generation (5G) wireless networks with a focus on propagation models," *IEEE Trans. Antennas Prop.*, vol. 65, no. 12, pp. 6213–6230, Dec. 2017.
- [14] F. H. Danufane, M. Di Renzo, J. De Rosny, and S. Tretyakov, "On the path-loss of reconfigurable intelligent surfaces: An approach based on Green's theorem applied to vector fields," *IEEE Trans. Commun.*, 2021, early access.